ELSEVIER

Journal of Nuclear Materials 240 (1997) 169–184

journal of nuclear materials

Fast diffusion in dilute binary alloys and its analysis based on Hägg's rule

Hubert Blank *

European Commission, European Institute for Transuranium Elements, P.O. Box 2340, D-76125 Karlsruhe, Germany

Received 5 September 1995; accepted 18 October 1996

Abstract

Fast solute diffusion in certain dilute binary alloys can be understood by a modified version of Hägg's rule. This method is substantiated and used to analyse published data on fast diffusion of (mainly) 3d-solutes in the anisotropic host phases β-U and α-Zr and to compare the results with those in bcc host phases. The activation enthalpy Q of fast diffusion consists of elastic contributions, ΔH_{el} and Δh_{el}, related to the Hägg parameter λ and a chemical one, ΔH_{cov}, due to the electronic solute-solvent interaction. For Fe, Co, Ni and O in α-Zr, ΔH_{cov} can be inferred from relevant solute–host phase diagrams. The Hägg-approach defines the geometrical frame within which fast solute diffusion occurs. To a certain degree it is complementary to the Miedema model which, however, is bound to neglect the structural details of the host lattice essential for interstitial diffusion.

1. Introduction

For about 30 years diffusional anomalies in two partly overlapping groups of metals have been studied. In the first group the anomalous phenomenon is enhanced self-diffusion in the lower temperature range of the bcc phase of β-Ti, β-Zr, β-Hf, γ-U and -Pu and of the metals Ce, Gd, La, Pr, and Yb, leading to curved Arrhenius plots of the coefficient of self-diffusion D_1^0 in those metals where the temperature field of the bcc phase is large enough. By convention (see, for example, Ref. [1]), the quantities D_1^0 and D_2^0 denote the tracer diffusion coefficients for self-(1) and impurity-(2) diffusion, respectively, in a pure host phase (1). D_1 and D_2 are the coefficients of the same tracers in the same host phase (1) containing larger concentrations c_2 of the impurity (2).

The second group partly overlapping with the first one constitutes the host metals for fast diffusion in certain dilute binary alloys and contains Ti, Zr, Nb, Hf, U and Pb. The fast diffusing solutes in these host metals are mainly 3d-metals but in part also Cu, Ag, Au and Cd. Fast solute diffusion in this group occurs in the isotropic, bcc and fcc phases as well as in anisotropic hcp and related phases. Comparing the two groups of metals it is obvious that the enhanced self-diffusion in the 'anomalous' bcc metal phases and the fast solute diffusion in the second group are two independent phenomena caused by different physical mechanisms. The present situation in the two fields can be characterized as follows.

The problem of the enhanced self-diffusion in the anomalous bcc metal phases has finally been solved during the last eight years by the work of Herzig and coworkers [2,3] and has been further quantified and evaluated subsequently by Vogl and Petri and co-workers using QNS (quasi-elastic neutron spectroscopy) and also QMS (quasi-elastic Mößbauer spectroscopy) as the main experimental tools [4] (see also, for example, Refs. [5,6]).

As regards the second problem, a considerable amount of experimental data has accumulated in the literature. Apart from the initial use of polycrystals the tracer technique was soon applied to anisotropic host phases and in hcp single crystals tracer diffusion parallel and perpendicular to the hexagonal axis was studied. In more recent times research concentrated largely on the fast diffusion of 3d-

* Present address: Erasmusstr. 12, D-76139 Karlsruhe, Germany.

PII S0022-3115(96)00712-X

metals in α-Zr single crystals since this metal phase is the basis of the technically important alloys zircalloy-2, -4 and Zr2.5Nb. The experimental difficulties encountered in this work have recently been outlined by Hood [7,8]. The application of the modern microscopic techniques QMS and QNS to fast diffusion has unfortunately certain limitations, restriction to $T < 380$ K and ambiguities in interpretation [9,10].

In the field of fast diffusion a geometrical frame is missing within which one could understand why certain solutes migrate by a fast (e.g., interstitial) diffusion mechanism and other ones show normal diffusion by the vacancy mechanism. Furthermore, the measured activation enthalpies have hardly been analysed. Attempts to establish such criteria on the basis of the Miedema model [11,12] were not entirely successful.

Therefore in a previous paper, Ref. [13], quoted in the following as part I, a new approach was developed. It takes account of the geometrical boundary conditions of the problem by a modified version of Hägg's rule. This method was used to establish empirical correlations between the Arrhenius parameter Q (activation enthalpy) of mainly 3d solutes in bcc host phases (γ-U, β-Zr and Nb) and the Hägg parameters λ (i.e., the ratio between solute and solvent radii) of these solutes in the respective host phases. In the present paper the empirical Hägg approach is extended to anisotropic host phases, substantiated further and applied to the qualitative analysis of fast diffusion in α-Zr and, as far as experimental data exist, β-U.

In Section 2 first the Hägg approach established in part I for a well defined class of dilute alloys is outlined and further elaborated and then the geometry of the interstitial sites in the host phases is described from the point of view of the hard sphere model (HSM). In Section 3, after a brief survey of the experimental situation fast diffusion in β- and γ-U is compared. The experimental results about fast diffusion of 3d-solutes in α-Zr are analysed on the basis of Section 2 and the contributions to the activation enthalpy Q are identified. In Section 4, after a survey about the experimental enhancement factors, various aspects of the interstitial diffusion mechanism are discussed mainly qualitatively on the basis of the Hägg model. Subsequently the model is compared with models applied previously to fast diffusion. In Section 5, the main results are summarized and some conclusions are drawn.

2. Hägg's rule and the geometry of interstitial sites

2.1. Modification of Hägg's rule to treat interstitial diffusion in dilute alloys

In part I the conclusions drawn from an early paper in this field, Ref. [14], have led to the following results.

(1) Fast diffusion is confined to a special class of dilute alloys. These are characterized by host phases of polyvalent ($z_o \geq 4$), electropositive metals and solute atoms with low valence ($z_i \leq 2$) and small ionic radii.

(2) Cubic host phases have to be described by the HSM with the model radius R_M defined via the bond length b by

$$R_M = b/2. \tag{1}$$

In the present paper this definition is extended to anisotropic host lattices: each atom in the unit cell may now have two or more bond lengths b_1, b_2, ..., corresponding to HSM radii R_{M1}, R_{M2}, ... By introducing the empirical parameters R_{M1} and R_{M2} for α-Zr the model takes care of the empirical and diffusion relevant fact that all hcp phases of the d-transition metals possess a contribution to anisotropy caused by a sizeable deviation $c/a < 1.6333$ (in contrast the hcp IIb-metals Zn and Cd possess $c/a > 1.6333$) from the ideal value 1.6333.

(3) The other key point of the Hägg analysis in part I is the fact that, specified on general electron theoretical arguments, the solutes must be described by their ionic radii $R_I(z_i)$ instead of metal radii, and if $R_I(z_i)$ satisfies Hägg's rule, [15], i.e., if

$$\lambda = R_I(z_i)/R_M < 0.59 \tag{2}$$

the ion will fit with tolerable lattice distortion into the interstice with its 'appropriate' ionic radius and charge $+z_i$, mostly for octahedral coordination with CN 6. The radii $R_I(z_i)$ can be taken from standard compilations of ionic radii. Comparing different published sets (see, for example, [16–20]), the slightly extended set of Ahrens [16] in [17] is preferred for the geometrically simple, dilute interstitial binary alloys discussed here. For oxygen in α-Zr the octahedral covalent radius of Ref. [21] has to be used.

(4) The relation $\lambda < 0.59$ is a necessary condition for interstitial diffusion.

When establishing in part I the empirical correlations between λ and the activation enthalpies Q of 3d solutes in bcc host phases several 'anomalies' in z_i were observed. These were resolved by assuming that Q has two contributions

$$Q = \Delta H_{el}(\lambda) + \Delta H_b. \tag{3}$$

The first term represents the saddle point energy for the elementary jump of the solute to its neighbouring interstice and has been related to λ by a provisional relation with λ assumed to be proportional to the saddle point strain and a constant C depending on the elastic constants of the solid and containing the volume of the interstitial,

$$\Delta H_{el}(\lambda) \approx C\lambda^2. \tag{4}$$

The second term ΔH_b, previously called ΔH_{cov} [13], describes the chemical solute–solvent interaction. However, since in addition it possesses a small elastic contribution it is better called the binding energy of the solute to its interstitial site, see Section 4.2.2.

Although the empirical and largely qualitative results in part I are consistent one would like to quantify them further and relate HSM of the host lattice and solute–solvent interactions to the electron theory of metals. However, here a fundamental difficulty is encountered. In the density functional theory [22,23] the lattice potential of the valence electrons is constructed with the muffin-tin geometry (for the Wigner–Seitz approach the situation is analogous). By this the crystal volume outside the muffin-tin spheres is attributed to valence electrons and regarded as 'interstitial volume' which includes also the real space of the interstitial sites defined by the HSM. Hence electron theory in this form is in conflict with the true interstitial space both in the undisturbed host lattice and in the host lattice with the interstitial ion.

A simple way of getting nevertheless some 'zeroth order information' on different host metals is to look at the valence electron states and their energies in the free host atoms, see Fig. 1 with data taken from Refs. [24,25]. Apart from Pb with $6s^2$ and $6p^2$ valence states the valence electrons of all transition metal hosts have states nd^2, $(n+1)s^2$ and in addition 5f electrons in U. For $n \geq 4$ the d- and s-levels are only ≤ 1 eV apart. This means for the metals overlapping bands with hybridization. The two valence s-electrons in each case may be taken to support the HSM.

Next, one can extend the 'zeroth order information' about the host lattice to the host–solute interactions by comparing the valence electron levels of the free host atom

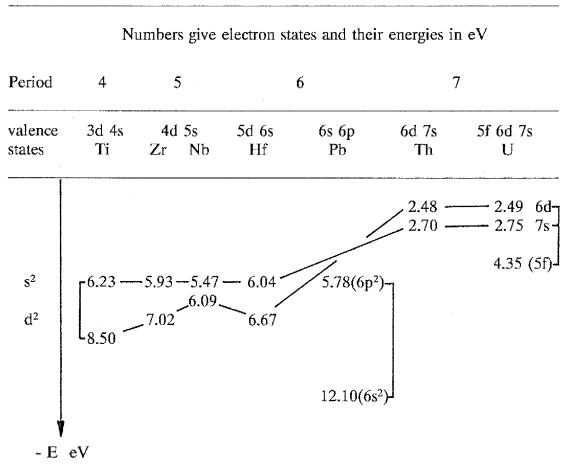

Fig. 1. Comparison between the valence states of the free host atoms of possible host metals for fast diffusion. With the exception of Pb the valence bands (marked by lines) of all other host metals are formed by s^2- and d^2-states which are closely spaced in energy. The valence band of Pb in contrast is formed by $6p^2$- and $6s^2$-states differing in energy by more than 6 eV.

with those of the free solute atoms. Valence states relatively close in energy for host and solute states are expected to combine and thus to take part in the host–solute interaction in the conduction and valence bands. From the semi-schematic presentation of the valence states of the

Table 1
Data of solute diffusion in the bcc host phases γ-U, β-U and α-U and the related parameters for their Hägg analysis: Host radii R_M, solutes, valences z, radii $R_I(z)$, Hägg parameters λ and Arrhenius parameters D_0, Q

Solute	z	R_I (nm)	λ	D_0 (cm²/s)	Q (eV)	T (K)	Ref.
(a) Host phase: γ-U, $R_M = 0.1535$ nm, $D_0 \approx 1.75$ cm²/s, $Q = 1.18 \pm 0.03$ eV							
Nb	1	0.100	0.686	5.5×10^{-2}	1.73		[34]
V	1	?	> 0.59		see Section 4.3		
	(2)	0.088	0.573	–	–		–
Cr	3	0.063	0.411	5.6×10^{-3}	1.06		[34]
Mn	2	0.080	0.521	2.0×10^{-4}	0.61		[34]
Fe	2	0.074	0.482	2.8×10^{-4}	0.53		[34]
Co	2	0.072	0.469	2.6×10^{-4}	0.51		[34]
Ni	2	0.069	0.450	6.7×10^{-4}	0.70		[34]
Cu	1	0.096	0.625	2.2×10^{-3}	1.06		[34]
Au	1	0.137	0.893	4.9×10^{-3}	1.32		[35]
(b) Host phase: β-U, $\bar{R}_M \approx 0.1603$ nm [a], $Q \approx 1.85$ eV [b], $D_0 \approx 1.4 \times 10^{-2}$ cm²/s [b] [36–38]							
Cr	2	0.089	0.56	$\approx 10^3$	≈ 2.4 [b]		[39,40]
Mn	2	0.080	0.50				
Fe	2	0.074	0.46	≈ 1 [b]	≈ 1.54 [b]		[39]
Co	2	0.072	0.45	1.5×10^{-3}	1.19		[40]
(c) Host phase: α-U, $\bar{R}_M \approx 0.1568$ nm [a]							
Co	2	0.072	0.459	1.0×10^{-10}		893	[40]
				1.75×10^{-10}		913	

[a] Value averaged over all bond lengths in the unit cell.
[b] Values averaged approximately over experimental data showing scattering due to non-quantified anisotropy.

free host atoms U and Zr and of the free solute 3d-atoms in Fig. 2 the following tendencies can be deduced.

(1) In γ-U the interaction between host and solutes should occur largely via the 5f-electrons of U and the s- and d-states of the 3d-elements. For 3d-solutes in Zr only d- and s-states are involved.

(2) The solute atoms Cr, Ni and Cu of the 3d-series are expected to show 'anomalies'. Especially for Cr the $4s^2$- and the $3d^5$-states are very dose to each other. This explains its anomalies in the effective valences (ionic radii) in Tables 1 and 2 (see also Ref. [17]) and in Figs. 3 and 4. Thus Cr behaves sensitively towards different host lattices.

(3) The situation for Cu is remotely similar, this means, besides its 'normal' valence s-electron even an electron of the complete d-shell might interact with the valence states of α- and β-Zr but not with the more remote 5f states of γ-U. For Ni the opposite seems to occur in γ-U. Because of its small ion radius only one s-electron may be given to the top of the Fermi distribution resulting in a somewhat higher λ-value as indicated in Fig. 3 by the arrow and the same may happen to V.

Hence in these cases effective valences z_e and associated ionic radii R_{Ie} may occur which differ from the 'normal' values $z_i = 2$ usually attributed to the 3d-elements. The at first sight surprising success of this zeroth order discussion of the electronic host–solute interaction becomes understandable if one remembers the fact that the electron theory of the d-transition metals has to be based on the (free-atom-like) tight-binding approximation (see, for example, [26]). Eventually one can combine the information from Figs. 1 and 2 for Pb as host. Here the interaction between host and solute is expected to occur at two levels separated mostly by 6 eV. At the first level the

Table 2
Data D_0 and Q of solute diffusion in the hcp host phase α-Zr and the related parameters for their Hägg analysis: HSM radii R_{M1}, R_{M2}, solute valences z, radii $R_I(z)$ and Hägg parameters $\lambda^{\|}$ and λ as well as temperature ranges

Solutes	z	R_I (nm)	λ	Q (eV)	T range (K)	D_0 (cm^2/s)	Ref.
Host α-Zr: $R_{M1} = 0.16156$ nm $R_{M2} = 0.15894$ nm							
Nb	1	0.10	0.635	(1.37p)			[42]
			$0.619^{\|}$				
V	2	0.088	0.558	0.99p	893–1123	1.12×10^{-8}	[43]
			$0.545^{\|}$				
Cr	1	0.081	0.514	1.61	890–1126	9.5×10^{-2}	[36,44]
			$0.501^{\|}$	$1.39^{\|}$		2.4×10^{-2}	
	2	0.089	0.565				
			$0.551^{\|}$				
Mn	2	0.080	0.508	1.31p	909–1111	2.4×10^{-3}	[53]
			$0.495^{\|}$				
Fe	2	0.074	0.470	1.09	1032–1133	6.7×10^{-2}	[45]
			$0.458^{\|}$	$0.925^{\|}$		6.6×10^{-2}	
				1.696	< 1000	62.5	
				$1.865^{\|}$		4.13×10^{3}	
Co	2	0.072	0.457	[a]	923–1070	[a]	[46]
			$0.446^{\|}$	[a]		[a]	
				1.83	826–923	1.2×10^{3}	
				$1.98^{\|}$	862–990	4.0×10^{4}	
Ni	2	0.069	0.438	0.65	> 1000	5.3×10^{-4}	[47,54]
			$0.427^{\|}$	$0.81^{\|}$		1.8×10^{-3}	
				2.14	882–1025		
				$1.915^{\|}$		6.75×10^{2}	
Cu	1	0.096	0.609				
			$0.594^{\|}$				
	2	0.072	0.457	1.60	888–1133	0.25	[48]
			$0.446^{\|}$	$1.54^{\|}$		0.40	
Ag	1	0.126	0.800				[49]
			$0.780^{\|}$	$2.54(^{\|})$	895–1117	2.20	
				2.18p		6.8×10^{-2}	
O	covalent	0.0737	0.468	2.12	630–870	0.49	[50]
			$0.456^{\|}$				
				2.38(p)	920–1770	16.5	[51,52]

Q-values marked by (p) pertain to diffusion in polycrystalline α-Zr.
Figures of λ and Q marked by $\|$ pertain to diffusion parallel and those without to diffusion perpendicular to the c-axis.
[a] Data not reliable.

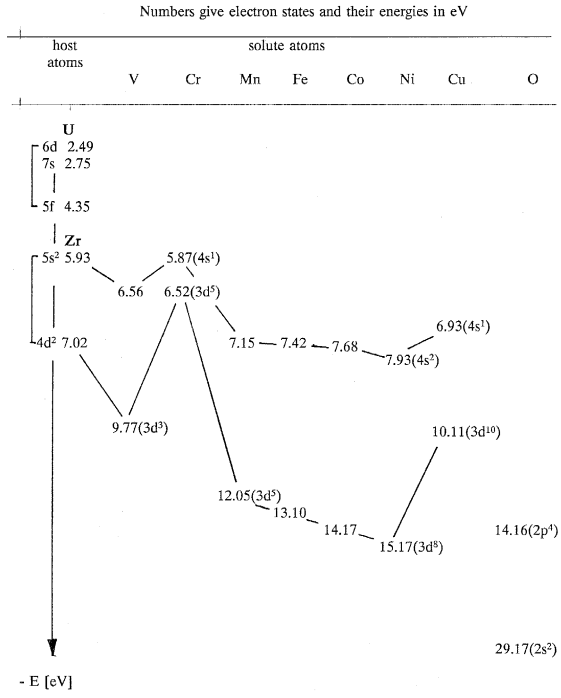

Fig. 2. Comparison between the semi-schematic atomic level scheme of the valence electrons in free host atoms Zr and U and the valence levels of free 3d-solute atoms and of oxygen. The same types of atomic levels are connected by lines. Note that for U as host the 5f-level is closest to the s-levels of the solute atoms. For details see Section 2.1.

$6p^2$-states of Pb combine with the s-electrons of Cu, Ag, Cd, Au and Ni and at the second one the $6s^2$-states of Pb possibly with the filled d-levels of Cu, Ag, Au and perhaps with $3d^8$ of Ni.

2.2. HSM and interstitial geometry in bcc, fcc and hcp (α-Zr) host phases

In spite of the ostensible 'text book character' of this section these crystal lattices have apparently not been discussed before from the point of view of interstitial diffusion on the basis of the HSM. It is emphasized that in the present context the HSM is based rigorously on Eq. (1) and its extension to anisotropic metals. Hence the empirical parameters R_{M1} and R_{M2} should not be confused with metallic radii and associated metallic valences in the literature.

2.2.1. The bcc lattice, HSM radius $R_M = (a/4)\sqrt{3}$, a = lattice parameter

(i) In the bcc lattice distorted tetrahedral interstices exist with two 'open' edges of length $l_1 = a$ and 4 edges with length $l_2 = 0.866a$. The radius of the interstice is $R_t = 0.291R_M$ [27] which is 30% larger than the tetrahedral interstices in the dose packed structures with $0.223R_M$.

(ii) The mirror planes of the octahedral interstices are defined by the cube faces of the unit cell and their apices by the body centered atoms. Consequently these interstices are strongly compressed along their symmetry axis, i.e along the ⟨100⟩ directions. In this way the interstice becomes anisotropic and has two widely differing radii, $R_{O1} = 0.633R_M$ and $R_{O2} = 0.154R_M$ in the mirror plane and perpendicular to it, respectively.

(iii) Contrary to the geometrical relations between octahedral and tetrahedral interstices in close packed structures

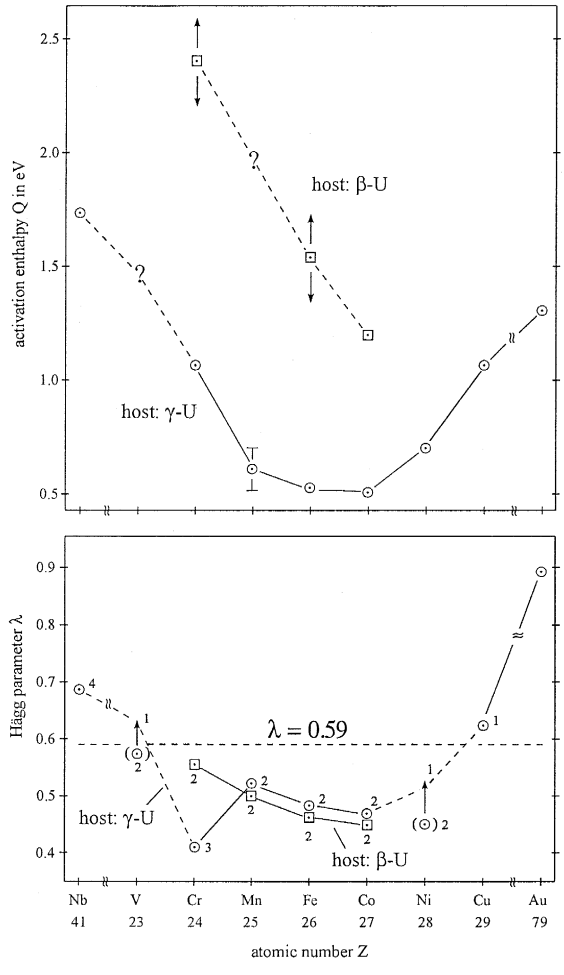

Fig. 3. Fast diffusion of 3d-solutes in β- and γ-U, data from Table 1a and b. Correlation of activation enthalpy Q (upper panel) and related Hägg parameters λ (lower panel) with the atomic number Z of the 3d-solutes on the abscissa for host phases β-U (squares) and γ-U (circles). Numbers at the λ-values indicate the effective valences of the solutes. Vertical arrows in the upper panel at Fe and Cr indicate scatter in Q due to non-quantified anisotropy in the polycrystalline host specimens. Valences and λ-values for β-U are tentative only. The critical Hägg parameter $\lambda = 0.59$ is indicated.

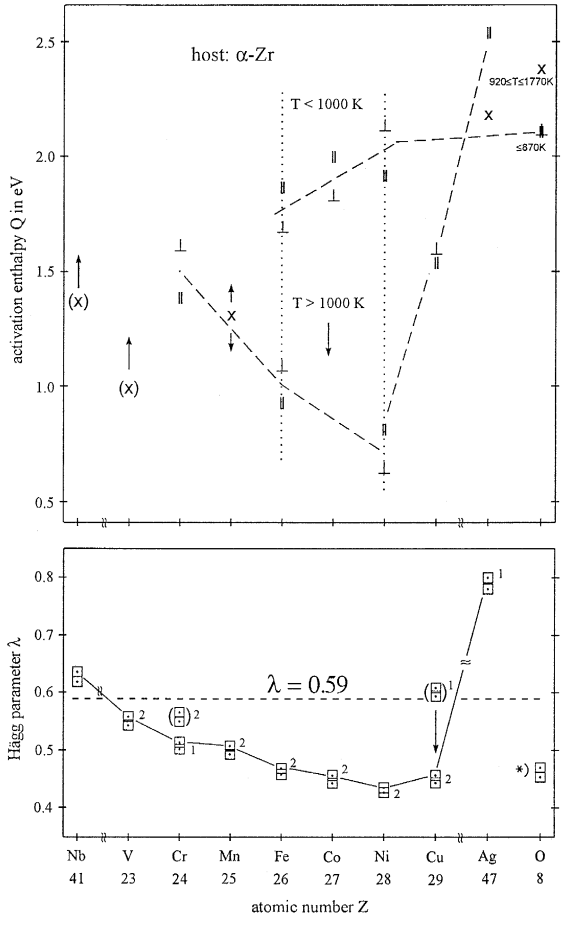

Fig. 4. Fast diffusion of 3d-solutes in α-Zr, data from Table 2. Correlation of activation enthalpy Q (upper panel) and of related Hägg parameters λ (lower panel) with the atomic numbers Z of the 3d-solutes shown on the abscissa. Q-values represented by crosses pertain to polycrystalline α-Zr specimens. Q-values obtained from single crystals show anisotropy with the symbols indicating solute diffusion perpendicular and parallel to the hexagonal c-axis, respectively. Also λ has two values, see Table 2. Numbers at the Hägg parameters indicate effective valences. The λ-values for oxygen are marked by $^{*)}$. Its Q-value for $T \leq 870$ K is at the level of the upper branch of the Q-values of Fe, Co and Ni valid at $T < 1000$ K. The lower branch valid at $T > 1000$ K shows normal Q-values. For further details see Section 3.3 and Section 4.2.4.

in the bcc lattice an octahedral site is *composed* of four tetrahedral ones.

Depending of the size of the interstitial solute these three properties have an interesting consequence for the accommodation of interstitials and their diffusion mechanisms.

(a) Interstitial ions with $0.291\,R_M < R_I < R_c$ (R_c defines a certain critical radius) will sit in tetrahedral interstices and require a static lattice distortion in which primarily the four tetrahedral lattice atoms are involved. For the elementary step of diffusion the interstitial will leave this site either via one of the four faces or across one of the two larger edges and jump into an adjacent tetrahedral site. In either case five lattice atoms will be involved, four of the old site and four of the new site with three atoms shared by both sites.

(b) Interstitials with radii $R_c < R_I < 0.59R_M$ are too big for displacing the four atoms around a tetrahedral interstice but they may use the octahedral hole by squeezing mainly the two body centred lattice atoms apart into the $\langle 100 \rangle$ and $\langle \bar{1}00 \rangle$ directions. Thus they will mainly enlarge the octahedral radius R_{O2} by forming a 'small crowdion' [29]. This may, however, be slightly asymmetrical the octahedral radius R_{O1} being somewhat too large in any case.

The theoretical determination of the critical radius R_c would require detailed lattice calculations involving crystal elasticity. Yet the analysis of diffusion data can serve to establish an empirical value of R_c, see Section 4.2.5.

2.2.2. The hcp lattice of α-Zr

The lattice geometry of hcp metals is well known (see, for example, [27,28]). The lattice parameters of α-Zr are $a = 0.32312$ nm and $c/a = 1.5931$ [30]. This gives two bond lengths b_1, b_2 for each lattice atom, $b_1 = a$ in the hexagonal basal plane and $b_2 = 0.31789$ nm between an atom in a basal plane and its nearest neighbors (n.n.) in an adjacent one. Thus for each atom of the host lattice there are two model radii R_{M1} and R_{M2} differing by 1.73% with 6 n.n. having R_{M1} and 6 n.n. R_{M2}. As a consequence in α-Zr the interstitial jumps of the solute within the (001) planes invariably involve only the smaller HSM radius R_{M2} of the host lattice whereas jumps parallel to the c-axis involve only the larger one, R_{M1}. This means in Eq. (2) that for the same solute ionic radius R_I the λ-value corresponding to the diffusion parallel to the c-axis, $\lambda^{\parallel}$, is systematically lower than the λ-value corresponding to diffusion within the (001) basal planes.

The ratio λ_O between the radius R_O of the octahedral site and R_M is of interest as reference for the Hägg parameter, Eq. (2). For this purpose the average HSM radius $\bar{R}_M = (b_1 + b_2)/4$ can be used giving for the octahedral interstices the ideal ratio which defines the lower limit for the

$$R_O/\bar{R}_M = 0.414. \tag{5}$$

Hägg parameters in the fcc and hcp structures.

The interstitial diffusion mechanism requires a solute ion to jump between adjacent octahedral positions. In the isotropic fcc host lattice two possibilities exist. (a) Via a two-step process the solute can leave its octahedral site parallel to a {111} plane across one of the eight faces of the octahedron, jump into an adjacent tetrahedral position and from there again across an octahedral face into the next octahedron. (b) In a one-step process the solute could leave the octahedral cage across a {110} edge forming a

small {110} crowdion at the saddle point configuration and jump directly into the adjacent octahedral site.

In the hcp lattice the geometry between two adjacent (001) atomic layers is identical with that of the interstitial sites between two adjacent {111} layers in the fcc lattice. Thus for the jumps of the hcp interstitial parallel to the (001) planes the mechanisms (a) and (b) can operate.

For diffusion perpendicular to the (001) planes another mechanism (c) specific to the hcp geometry works: (c) here chains of octahedral sites exist parallel to the *c*-axis which share common faces. The saddle point configuration is attained in this case by squeezing the three lattice atoms apart which represent the face shared by two adjacent octahedral cages on top of each other.

Thus the anisotropy of solute diffusion in α-Zr will have two contributions.

(i) The difference between the Hägg parameters λ and $\lambda^{\|}$ for solute jumps parallel to the hexagonal planes and parallel to the *c*-axis, respectively, because of the two HSM radii R_{M1}, R_{M2}, and

(ii) the differences between the mechanism (c) operating parallel to the *c*-axis and mechanisms (a), (b) operating within the hexagonal planes. These geometrical details will be required in Section 4.2.4.

2.2.3. Lattice structure of β-U

Recently [31] the complicated tetragonal structure was confirmed to be practically identical with the σ-phase [32]. From a general structural point of view β-U and the σ-phase belong to the family of the 'Frank Kaspar structures' of interpenetrating polyhedra [30,33]. In these structures space filling is attained by a distorted tetrahedral packing of atoms. The coordination number is 14 and there seem to be no octahedral interstices in contrast to the simpler cubic and hexagonal structures. The structure is compressed along the *c*-axis. In view of the large variety of bond lengths [31] an average bond length $\bar{d}$ with the associated average HSM radius $\bar{R}_M$ has been deduced, see Table 1(b).

3. Analysis of experimental results on fast diffusion

3.1. General situation about the experimental data on fast diffusion

Concerning the fast tracer diffusion in the isotropic bcc and fcc host phases no special problems have been reported, the primary solid solubility of the tracers being relatively high in the bcc phases. Grain boundary diffusion apparently was not found to affect the diffusion data. As observed in part I this situation results in reliable values of both Arrhenius parameters D_0 and Q.

The experimental situation for α-Zr is different due to anisotropy and in part very restricted solid solubilities just at the technologically interesting lower temperatures. Because of the related difficulties and complications [7,8] and in spite of a considerable amount of data there is nevertheless a certain lack of systematic studies from the point of view of the present paper.

For the quantitative analysis via Hägg's rule ideally one would like to have reliable $D_2^0(T)$ values between 750 and 1136 K determined from high purity α-Zr single crystals oriented parallel and perpendicular to the *c*-axis which cover systematically all 3d-solutes from V to Ni and in addition Cu, Ag and oxygen. Such an ideal data set could provide quantitative relations between Hägg parameters λ and the Arrhenius parameters D_0 and Q and possibly result in a classification of different diffusion mechanism similar to the results from the bcc phase in part I [13]. The limitations of the advanced microscopic methods QMS and QNS give results which are in part difficult to interpret [9,10].

As regards the anisotropic β-U host phase only the solutes Cr, Fe and Co have been investigated [39,40]. Because of experimental difficulties (anisotropy, narrow temperature range, 941–1048 K, diffusion experiments only with polycrystalline specimens) the data on Cr and Fe carry large errors. Nevertheless, alone the fact that fast diffusion exists in this strongly covalent, complicated crystal phase is of considerable interest.

3.2. Comparison of the behavior of 3d-solutes between γ-U and β-U host phases

In Table 1(a) and (b) the necessary information about the experimental diffusion data, attributed ionic radii $R_I(z)$ and related Hägg parameters $\lambda(z)$ in the two host phases has been collected. In Fig. 3 the activation enthalpies Q (upper panel) and the related Hägg parameters following Eq. (2) (lower panel) have been plotted versus the atomic numbers Z on the abscissa for the 3d-solutes in β- and γ-U. At the left and right ends results of two solutes, Nb and Au respectively, with other Z-numbers are shown. Of these Nb does not belong to the Hägg class of solutes defined in Section 2.1 and Ref. [14] but is nevertheless shown in Table 1(a) and in Fig. 3 for comparison.

Solutes in γ-U with Hägg parameters $\lambda > 0.59$ show high Q-values, dissolve substitutionally and migrate by the vacancy mechanism. Though diffusion data for V is missing by analogy to V in β-Zr (see Table 3(a) and Fig. 3), it is likely that V will show $\lambda > 0.59$ in γ-U and diffuse by the vacancy mechanism as well. The solutes from Cr to Ni show $\lambda < 0.59$, dissolve interstitially, possess low Q-values (with the exception of Cr) and diffuse by interstitial mechanisms. Thus Hägg's rule is satisfied. Cr behaves exceptionally showing an anomalously high valence, low λ and high Q. The anomaly of Ni is less obvious. Apart from Cr in γ-U a correlation between λ and Q following Eq. (4) may be suggested. The anomalies of Cr and Ni in γ-U may be understood from Section 2.1 and Fig. 2.

Of the three Q-values available for the host phase β-U,

Cr and Fe carry relatively large errors, see vertical arrows in Fig. 3, because of the unspecified pronounced anisotropy in the host phase [36–38]. On the contrary, the behaviour of Co is anomalous since it does not respond to the anisotropy of the polycrystalline, large grained specimens and its Q-value is rather precise. In spite of these differences in precision, Fig. 3 and Table 1(b) show that the Q-values of Cr, Fe and Co in β-U are roughly the double of the values in γ-U, see also Section 4.2.3. Though further interpretation appears rather speculative on the basis of the available data, these results in β-U deserve attention because

1. Their enhancement factors are relatively high, see Section 4.1.
2. Cr appears to be the only solute with a certain solubility in β-U which stabilizes this phase sufficiently that it can be quenched to room temperature and be kept there without loss of mechanical stability [41].
3. The β-U phase is rather densely packed, apparently without octahedral interstices and possesses a strong covalent and anisotropic bonding not otherwise encountered in pure metals.
4. The two D_2^0-values of Co in α-U in Table 1c are discussed in Section 4.1.

3.3. Analysis of fast solute diffusion in α-Zr

In Table 2 the data corresponding to Table 1 have been collected for the host phase α-Zr and in Table 3(a) for β-Zr. The activation enthalpies Q and the associated λ-values for α-Zr are plotted in Fig. 4 similar as in Fig. 3 for the uranium phases. The Q-values of polycrystalline samples are represented by crosses and those obtained in single crystals by symbols marking diffusion parallel and perpendicular to the hexagonal c-direction, respectively. At the left side of the abscissa Nb is shown as in Fig. 3 but at the right end Au is replaced by Ag and the non-metal O. The recent single crystal measurements of O in α-Zr [50] did not reveal a noticeable anisotropy in Q. As discussed in Section 2.2 and shown in Table 2 there are two slightly different λ-values in α-Zr. The effects related to anisotropy in Figs. 3 and 4 are discussed in Section 4.2.4.

In spite of the difficulties outlined in Section 3.1 the experimental data available on single crystal α-Zr can be

Table 3
Data of solute diffusion in the host phases β-Zr, Nb and Pb and the related parameters for their Hägg analysis: Host radii R_M, solutes, valences z, ionic radii $R_I(z)$, Hägg parameters λ and Arrhenius parameters D_0 and Q

Solute	z	R_I (nm)	λ	D_0 (cm^2/s)	Q (eV)	T range (K)	Ref.
(a) Host phase: β-Zr, $R_M = 0.1569$ nm							
Nb	1	0.100	0.637	9.0×10^{-6}	1.27	1174–2020	[55]
				7.4×10^{-2}	2.23		
V	1	?	> 0.59	7.6×10^{-3}	1.99	1140–1470	[43]
				0.3	2.49	1470–1670	
	2	0.088	0.560				
Cr	1	0.081	0.516	7.0×10^{-3}	1.478	1187–1513	[58]
Mn	2	0.080	0.510	5.6×10^{-3}	1.435		[53]
Fe	2	0.074	0.471	7.4×10^{-3}	1.12		[29,57]
Co	2	0.072	0.458	3.3×10^{-3}	0.95	1193–1970	[29,56]
Ni	2	0.069	0.438	–	–		
Cu	1	0.096	0.608	–	–		
Ag	1	0.126	0.804	4.2×10^{-4}	1.37	1200–2000	[59]
				190.5	3.36		
U	4	0.097	0.618	7.8×10^{-5}	1.12	1188–1470	[60]
(b) Host phase: Nb, $R_M = 0.1432$ nm							
V	2	0.088	0.614	2.21	3.70		[43]
Fe	2	0.074	0.517	0.14	3.06		[61]
Co	2	0.072	0.503	0.11	2.85		[61]
Ni	2	0.069	0.482	0.077	2.74		[61]
U	4	0.097	0.677	0.089	3.34		[60]
(c) Host Phase: Pb, $R_M = 0.175$ nm, $D_0 = 0.46$ cm^2/s, $Q = 1.078$ eV							
Cu	2	0.072	0.411	7.9×10^{-3}	0.35		[62]
Au	3	0.085	0.486	4.1×10^{-3}	0.41		[63]
Ni	1	?	?	1.1×10^{-2}	0.47		[62]
Ag	2	0.089	0.508	4.6×10^{-2}	0.628		[62]
Cd	2	0.097	0.543	4.1×10^{-2}	0.923		[64]

The R_M values of β-Zr and Nb are based on the lattice parameters at 1520 and 1570 K, respectively, amidst most of the diffusion data.

used for further analysis in the following and as regards $\Delta H_{el}(\lambda)$ in a wider context in Section 4.2.3.

3.3.1. General results

From Fig. 4 the following general results can be deduced.

(1) With the exception of Nb and Ag which clearly show $\lambda > 0.59$ and a less reliable early polycrystalline result on V (which has λ rather close to 0.59) all other solutes possess $\lambda < 0.59$ and thus migrate by interstitial mechanism(s) as can be verified by consulting the literature cited in the last column of Table 2.

(2) There is a correlation between the lower curve of Q versus Z and the curve λ versus Z in the bottom part of Fig. 4 with the exception of Cr, Cu and the non-metal O.

(3) The three iron group solutes, Fe, Co and Ni, possess two branches of the Q-values. The lower branch pertaining to $T > 1000$ K shows, as far as the data exist, regular behavior in the relation between Q and λ. In contrast the upper branch valid at $T \leq 1000$ K clearly has to be associated with a different diffusion mechanism with distinctly higher Q-values.

(4) The 'irregularities' of Cr and Cu (both identified in the experiments as interstitial diffusers) are associated with the fact, that in both cases the 'normal' valence would not correlate with Q and the diffusion mechanism like for Cr and Ni in Fig. 3. The reasons are found in Section 2.1 and Fig. 2.

(5) The Q-value of oxygen at the extreme right of Fig. 4 valid at $T \leq 870$ K is comparable with the upper Q-branch of the iron group metals valid in the same low T-range. In all these cases high activation enthalpies Q combine with low λ-values and are associated with the interstitial mechanism.

The general results, items (1), (2), and the high temperature results of (3) demonstrate that the Hägg analysis of fast solute diffusion in α-Zr yields a correlation between Hägg parameter λ and Q as indicated by Eq. (4) only for Fe, Co and Ni and perhaps still for Mn. Regarding the diffusion behavior of Cr and Cu, the low temperature behavior of the iron group solutes and of oxygen, the Q-values have to be expressed by Eq. (3) and the term ΔH_b for the chemical (electronic) solute–solvent interaction makes a higher contribution to Q than the elastic saddle point energy $\Delta H_{el}(\lambda)$.

3.3.2. The origin of ΔH_{cov} in the term ΔH_b

There are at least two different causes for the chemical solute–solvent interaction, ΔH_{cov} one works via 'anomal, effective valences z_e' of the solute ions and one via the formation of intermetallic compounds.

(i) 'Anomal, effective valences z_e'. Apart from the case of Ni in γ-U this effect can be explained if for $z_e > z_i$ not all valence electrons of the solute are given to the top of the Fermi distribution and the balance $z_e - z_i$ is used for local bonding with host atoms. This appears possible on the basis of Fig. 2 in Section 2.1. Thus the different behaviour of Cu in γ-U (vacancy mechanism) (see Fig. 3) and in α-Zr (interstitial mechanism [48]), see Fig. 4, may be attributed to the large (≈ 6 eV) separation of the occupied 3d-levels of Cu from the 5f-level in U and the smaller (≈ 3 eV) difference between 3d- and 4d-levels in Zr leading to the interaction between these two d-levels and hence the effective valence $z_e = 2$ for Cu in α-Zr. It is suggested that the same should also apply to Cu in β-Zr though no experimental data exist in this case. As mentioned in Section 3.2, following Fig. 2, Cr is especially prone to this mechanism.

Table 4
Terminal solid solubilities (TSS), eutectoid reaction isotherm T_e and first intermetallic compounds in α- and β-Zr-solute systems [a]

α-Zr					β-Zr			
Solute	$\lambda^{\parallel}$	TSS (at.%)	T_e (K)	compound	T_p (K)	λ	TSS (at.%)	Ref.
Nb	0.62	0.6	890	–		0.637	100	[65]
V	0.559	≤ 1.0	1050	ZrV_2	1570	0.56	≈ 17	[66]
Cr	0.501	≈ 0.4	1104	$ZrCr_2$	1950	0.516	≈ 8	[67]
Mn	0.495	?	1068	$ZrMn_2$	1610	0.51	10	[68]
Fe	0.458	1.4e − 2	1065	Zr_3Fe	1158	0.471	≈ 6.5	[69,70]
			1000					[71,72]
Co	0.446	1.4e − 3	1106	Zr_2Co	1370	0.458	3.4	[73,74]
Ni	0.427	1.4e − 3	1118	Zr_2Ni	1390	0.438	≈ 3	[74,75]
Cu	0.446	≈ 0.2	1095	Zr_2Cu	1300	0.608	≈ 6	[76]
O	0.456	25	2400 [b]	Zr_3O	2240	–	≤ 10	[77]
Ag	0.780	1.6	1093	Zr_2Ag	1464	0.804	20	[78]
Au	0.86	< 1	1093	Zr_3Au	≈ 1470	0.874	≤ 10	[79]
U	–	≤ 0.31	1136	Zr_2U	880	0.618	100	[80]

[a] Transition temperature: $T_{\alpha/\beta} = 1136$ K; eutectoid reaction isotherm T_e: β-Zr = α-Zr + Zr_yM_x; TSS = terminal solid solubility of solute in α-Zr at $T \approx T_e$; T_p = peritectoid.
[b] Melting point.

(ii) Formation of intermetallic compounds, systems Zr–O and Zr–Fe. The combination of the low value $\lambda \approx 0.46$ for oxygen in Fig. 4 with the high value $Q = 2.12$ eV finds a simple explanation in the Zr-rich side of the binary phase diagram Zr–O whose relevant data has been collected together with the data from other Zr-3d-solute phase diagrams and some other solutes in Table 4. This data represents the terminal solid solubility (TSS) in the α-Zr phase at the eutectoid reaction isotherm T_e and the first Zr-rich compound in each binary system with its peritectoid decomposition temperature T_p. In the Zr–O system T_e and T_p had to be replaced by the melting temperature of Zr_3O. The difference of T_e with regard to the α/β transformation at 1136 K indicates how much a solute stabilizes either the α- or the β-phase of Zr.

As regards oxygen the α-Zr phase is stabilized in a dramatic way by raising the α/β transformation temperature from 1136 K of pure Zr to a melting temperature of 2400 K if the interstitial oxygen concentration is increased from zero to around 25 at.% corresponding to the composition Zr_3O. This effect is explained by the fact that an oxygen atom in an octahedral interstice makes covalent bonds with its 6 Zr nearest neighbors, or in other words, the complexes (O + 6Zr) form stable structural units within the α-Zr(O) phase [81]. For interstitial diffusion the 6 covalent O–Zr bonds constituting the largest part of the contribution ΔH_b in Eq. (3) have first to be broken before the oxygen atom can be activated to perform its jump towards a neighboring empty octahedral site with the activation enthalpy $\Delta H_{el}(\lambda)$.

The case of Fe in α-Zr is partly different. Indeed, the system α-Zr–Fe shows also a strong solute–solvent interaction energy as indicated by the Zr-rich compound Zr_3Fe but otherwise properties opposite to the system Zr–O, see Table 4.

(i) Fe stabilizes the β-Zr phase, i.e., lowers the α/β transformation temperature and the degree of this lowering apparently is still a matter of debate. Following Refs. [71,72] it is proposed that the higher T_e value used by Refs. [69,70] could stem from the stabilization of the α-phase by oxygen impurity.

(ii) Fe, similar as Ni and Co, has an extremely low terminal solid solubility in α-Zr. Hence for $T \leq T_e$, Fe is practically always precipitated as Zr_3Fe.

Analogous to the oxygen complexes these precipitates have to be broken up by providing an energy ΔH_{cov} before the Fe-ions can make the elementary interstitial jump involving the elastic saddle point contribution $\Delta H_{el}(\lambda)$. As emphasized repeatedly [7,8,82] these properties of iron provide serious difficulties in α-Zr in determining reliable solute diffusion and self-diffusion data. Without doubt, the strong solute–solvent interactions of the elements oxygen and nitrogen (which behaves like oxygen) always present as impurities in α-Zr, will also contribute to these difficulties.

Thus the low temperature branch for the activation enthalpies of the three irongroup elements in Fig. 4 finds its explanation in the solute–solvent interaction term ΔH_b of Eq. (3) and the related TSS data and intermetallic compounds of Table 4.

4. Discussion

4.1. Enhancement factors of fast diffusion in various host phases

A survey on the relative magnitudes of fast diffusion in various host phases is given in Table 5. The enhancement factor f_i is defined by the ratio of the coefficients for tracer diffusion D_2^0 and for self-diffusion D_1^0, $f_i = D_2^0/D_1^0$ and may vary by factors of the order of 10 between the lower and upper limit of the useful temperature range in a given host phase. Here only the approximate orders of magnitude of f_i are of interest. In Table 5 the f_i-values of (a) the fastest diffusing solutes, Fe and Co and (b) the f_i values of the 'slow' solute Cr arc shown for the phases of the transition metals U, Zr and Nb. The example Cr is used because of the variable effective valence of this solute, and Cu behaves similarly. As a general tendency one finds the highest enhancement in the phases existing at the lowest temperatures. For the general possible occurrence of fast diffusion it is worth noting that in spite of strong anisotropy and the high covalent contribution to bonding in α-U and especially in β-U the solutes Fe and Co possess roughly the same enhancement factors as in Nb. Furthermore γ-U and β-Zr behave as rather similar hosts for the 3d-solutes. In contrast to the f_i factors of Table 5 the maximum enhancement of self-diffusion in the 'anomalous' bcc phase β-Zr near the bcc/hcp transition is only about 10.

Table 5
Enhancement factors f_i for fast diffusion of Fe, Co and Cr in various host phases

Host phases	Solutes			T (K)
	Fe/Co	Cr		
α-U	–/2300	–		920
β-U	2000/2000	140		980
γ-U	130/130	13		1176
α-Zr	$3\times10^8/3\times10^8$	10^6		1110
β-Zr	210/380	10		1428
Nb	400/1500	–		1400
Host phases	Solutes			T (K)
	Cu	Ag	Cd	
Pb	1.6×10^5	1.9×10^3	30	520

4.2. Properties of the Hägg model

Following Eq. (3) the Hägg model provides for the first time the means to identify the elastic (lattice dynamic) and electronic contributions to the activation enthalpy Q for fast diffusion. Hence the combination of the results from crystal elasticity and electron theory of metals is required to quantify the model. This is beyond the scope of the present paper. However, some qualitative aspects and properties of the model can be outlined.

4.2.1. The tolerable static lattice strain in dilute interstitial alloys

The static lattice strain caused by a solute ion located on an octahedral interstice of a close packed fcc or hcp host lattice may be compared with the well known 15% rule of Hume–Rothery for substitutional solid solubility. Following Eq. (5) the lower limit of λ (zero distortion) is given by λ_0 and the upper limit λ_m at 15% radial strain by the relation $(\lambda_m - \lambda_0)/\lambda_0 = 0.15$. This leads to the following range of the Hägg parameters within the 15% rule

$$0.414 \leq \lambda \leq 0.476 \quad (6)$$

for dilute alloy systems with close packed host lattices showing fast diffusion. Following Figs. 3 and 4, see also Tables 1 and 2, this range is indeed mostly respected. Only in the 'open' bcc host lattices is $\lambda_m = 0.48$ to 0.52 observed [13]. Yet, in close packed host phases $\lambda_m \approx 0.50$ may also occur corresponding to about 20% radial strain. The strain parameter

$$= (\lambda - \lambda_o)\lambda_0 \quad (6a)$$

can be used to estimate the related strain energy. In a simplified approximation one obtains with the assumption that the interstitial ion is much harder than the matrix

$$\Delta h_{el}(\lambda) \approx 6 G_m V_0^{\ 2} \quad (6b)$$

with G_m shear modulus of the matrix and V_O the volume of the octahedral site. From this relation one gets Δh_{el} of the order of 0.01 eV in α-Zr.

4.2.2. The binding energy ΔH_b of the solute to its interstitial site and the interaction with a lattice vacancy

The static elastic strain energy $\Delta h_{el}(\lambda)$ of Eq. (6b) has to be added to the covalent solute–solvent interaction enthalpy ΔH_{cov} to obtain the binding enthalpy of the ion to its interstitial site, hence

$$\Delta H_b = \Delta h_{el} + \Delta H_{cov}. \quad (7)$$

Eq. (7) has the consequence that apart from an electronic effect mutual attraction exists between the interstitial ion and a nearby lattice vacancy. To quantify the possible interactions between the interstitial solute and the vacancy, following Le Claire [1], jump frequency models are required for the hcp α-Zr lattice to analyse the competing geometries of interstitial and substitutional solution and diffusion and the possibilities of an interstitially mechanism. In this context the interaction between interstitial oxygen and the mobility of lattice vacancies in α-Zr and an α-Zr–1%Nb alloy should be mentioned [83] as well as the interaction of Fe with lattice vacancies in the temperature ranges $T < 1000$ K and $T \geq 1000$ K [84–86]. These points deserve a separate investigation which is beyond the present analysis.

4.2.3. The saddle point energy $\Delta H_{el}(\lambda)$ and the elastic properties of the host phases

In the saddle point term ΔH_{el} of Eq. (4) the quantity C had been related to the elastic properties of the respective host phases and these may be represented by their bulk moduli B. By choosing in all host phases the same solutes for which one can assume in Eq. (3) $\Delta H_{el} \gg \Delta H_b$ one can replace in Eq. (4) ΔH_{el} by Q and the following relation should approximately hold

$$B \approx Q/\lambda^2 \quad (8)$$

for $\Delta H_{el} \gg \Delta H_b$. The solutes for which this relation should be valid in *all* host phases are primarily Fe and Co whereas it may hold for Cr, Mn and Ni only in certain host phases due to different contributions of ΔH_{cov} in Eq. (7).

In Table 6 the relevant solutes, their Q/λ^2 values and the corresponding values of bulk moduli B are shown for each host phase. The modulus B has not yet been determined for γ-U but it is known to be very low [87,88], of the order indicated. Young's modulus E and shear modulus G have been determined for β-U. The deduced value of B is certainly much higher than in γ-U, but with the experimental difficulties encountered in the measurement of E and G [88] it is subject to a large error. In contrast to

Table 6
Analysis of the elastic term $\Delta H_{el}(\lambda)$ following Eqs. (4) and (6a) in the host phases of U, Zr and Nb by comparison with the bulk moduli B of these phases at relevant temperatures T

Phase	α-U	β-U	γ-U	β-Zr	α-Zr	Nb
T (K)	920	1010	1100	1250	1000	1570
Solutes	Co	Fe, Co	Mn, Fe, Co	Cr, Mn Fe, Co	Cr, Mn Fe	Fe, Co Ni
B (GPa) [b]	100	(≈ 200)	(≈ 20)	≈ 75 [a]	88.5	≈ 155 [a]
Q/λ^2 (eV)	?	5.9–7.1	2.3	4.5–5.5	4.5–5.5	11.25–11.75

[a] Extrapolated and taken from graphs of Ref. [90], respectively.
[b] The bulk moduli B of β- and γ-U are rough indications only, see text.

uranium the bulk moduli do not differ very much between α- and β-Zr [89,90] and for Nb the quantity B is roughly a factor of 2 higher than for Zr. The last two lines in Table 6 show the values of Q/λ^2 and B to fit Eq. (8) approximately. This rough correlation is less precise than the $cB\Omega$ method of Varotsos and Alexopoulos [91] but is regarded here as sufficient because of the neglect of and the missing information on the term ΔH_{cov}.

4.2.4. The quantities $\Delta H_{el}(\lambda)$, ΔH_{cov} and anisotropic fast diffusion in α-Zr

The anisotropy in the Arrhenius parameters D_0 and Q can be investigated on the basis of the Hägg model. Yet, the experimental scatter in the preexponential factor D_0, see Section 3.1, prevents the detailed analysis and only Q and $Q^{\parallel}$ of Table 2 and Fig. 4 will be discussed.

(a) Anisotropic diffusion of Fe, (Co) and Ni at $T > 1000$ K. The analysis is based on Eqs. (3) and (4) and on the difference $\Delta Q = Q - Q^{\parallel}$ of the Q values measured perpendicular and parallel to the c-axis in α-Zr (see Table 2). For the present estimation the small contribution Δh_{el} (Eq. (6b)) in ΔH_b and a small correction in ΔH_{el} due to the difference between λ and $\lambda^{\parallel}$ is neglected and the difference ΔQ is written simply

$$\Delta Q = \left[\Delta H_{el}(\lambda) - \Delta H_{el}(\lambda)^{\parallel}\right] + \left[\Delta H_{cov} - \Delta H_{cov}^{\parallel}\right]. \quad (9)$$

If the geometric anisotropy of the α-Zr structure described in Section 2.2.2 dominates one has $\Delta H_{el} > \Delta H_{el}^{\parallel}$. For normal valence of the solute one can assume that $\Delta H_{el} \gg \Delta H_{cov}$ and $\Delta H_{el}^{\parallel} \gg \Delta H_{cov}^{\parallel}$ and from Table 2 follows for Fe at $T > 1000$ K the relation $\Delta Q = Q - Q^{\parallel} > 0$ or

$$\Delta Q \approx \Delta H_{el} - \Delta H_{el}^{\parallel} \approx 0.16 \text{ eV}. \quad (9a)$$

The reverse anisotropy for Ni at $T > 1000$ K, see Table 2 and Fig. 4, must then be caused by two effects: (i) the migration enthalpies in the first bracket of Eq. (9) have to be relatively small, i.e., smaller than for Fe, and (ii) the second bracket of Eq. (9) must be sufficiently negative. Thus $\Delta H_{cov}^{\parallel} > \Delta H_{cov}$, and the bonding of the Ni-ion in the octahedral site must be stronger parallel to the c-axis than perpendicular to it in order to overcompensate the geometrical anisotropy.

(b) Anisotropic diffusion of Fe, Co and Ni at $T < 1000$ K. For $T < 1000$ K the situation is exactly reversed, i.e., $\Delta Q = Q - Q^{\parallel} < 0$, and in fact the anisotropy in the terms ΔH_{cov} and $\Delta H_{cov}^{\parallel}$ must be considerable. It should now be related to the existence of the corresponding intermetallic compounds in Table 4. To estimate ΔH_{cov} and $\Delta H_{cov}^{\parallel}$ for Fe in Eq. (9) the following argument is used: for Fe the enthalpies of migration above and below 1000 K should be the same, see Eq. (9a). Hence, subtracting them from Q and $Q^{\parallel}$, respectively, at $T < 1000$ K will give approximately ΔH_{cov} and $\Delta H_{cov}^{\parallel}$ at $T < 1000$ K. The result for Fe at $T < 1000$ K is $\Delta H_{cov} \approx 0.605$ eV and $\Delta H_{cov}^{\parallel} \approx 0.94$ eV and their difference is $\Delta H_{cov} - \Delta H_{cov}^{\parallel} \approx -0.33$ eV.

(c) Solutes showing no anisotropy, $\Delta Q \approx 0$, O in α-Zr and Co in β-U. Following the recent careful measurements of oxygen diffusion in α-Zr at $T \leq 870$ K [50] it must be assumed on the basis of the above analysis that the result $\Delta Q \approx 0$ is attained by compensation of the geometrical anisotropy with a similar but opposite covalent one in the octahedral complexes (O + 6Zr). This is quite possible in α-Zr. Comparison of Fe and O in Table 2 shows that both solutes have practically the same value of λ. Hence, based on the situation for Fe under (a) one can deduce from Eqs. (9) and (9a) for O with $Q = 2.12$ eV and $\Delta Q \approx 0$ between 500 and 1136 K reasonable values of the four quantities in Eq. (9), $\Delta H_{el} \approx 1.1$ eV, $\Delta H_{cov} \approx 1.02$ eV and $\Delta H_{el}^{\parallel} \approx 0.95$ eV, $\Delta H_{cov}^{\parallel} \approx 1.17$ eV. The fact that Co in β-U, see Fig. 3 and Table 1(b), does not show any anisotropy may be explained by an analogical mechanism.

4.2.5. Two fast diffusion mechanisms in bcc host lattices

When plotting the Arrhenius parameters D_0 and Q from the diffusion in samples with basically the same structure but different compositions in a common $\log D_0$–Q diagram one finds that samples showing different diffusion mechanisms are located on different straight lines. In part 1 this method was applied to the D_0 and Q parameters of the 3d-solutes in γ-U and β-Zr of Table 1(a) and Table 3(a), respectively. Plotting the systems from both host phases with $\lambda < 0.59$ in a common $\log D_0$–Q diagram gives two straight lines, one with Hägg parameters in the range $0.42 \leq \lambda \leq 0.49$ and the other one with $0.51 \leq \lambda \leq 0.53$. In part I these two curves were attributed to 'interstitial diffusion' and 'vacancy aided interstitial diffusion', respectively. The more detailed discussion of the interstitial sites in the bcc structure of Section 2.2.1 allows for a clarification of this interpretation. In fact, the mechanism associated with the range of the smaller λ-values should belong to the solutes sitting in tetrahedral sites and the mechanism correlating with the larger λ-values to solutes in octahedral sites. Consequently, the critical solute radius R_c defined in Section 2.2.1 is thus found to be $\lambda_c \approx 0.50$.

For fast diffusion in the bcc host metal Nb, see Table 3(b), the Hägg model predicts that Ni with $\lambda < 0.50$ uses the tetrahedral interstices and Fe and Co with $0.59 > \lambda > 0.50$ the octahedral ones.

4.3. Diffusion of 3d-solutes and oxygen in α-Ti and α-Hf

From the comparison of the relevant binary phase diagrams the following general statements and predictions can be made about the diffusion behaviour of 3d-solutes and oxygen in the three group IV solutes α-Ti, [92], α-Zr and α-Hf.

(a) The Hägg parameters in α-Ti and α-Hf are nearly the same as in α-Zr.

(b) The system Fe–Zr is an exception within the 3d-solute-group IV solvent systems. It is the only system with a solvent-rich intermetallic of type Zr_3Fe together with very low solubility at $T < 1000$ K.

(c) Oxygen forms octahedral structural complexes (O + 6M) with strong bonding in all three host metals. In α-Hf, however, the bonding in the complex (O + 6Hf) is stronger than in (O + 6Ti) and (O + 6Zr).

Based on these three observations it is to be expected that the diffusion behaviour of 3d-solutes (self-diffusion, vacancy and interstitial mechanism) in the three group IV metals is very similar with the exception of possible special effects related to Fe in α-Zr. Oxygen should affect the diffusion behaviour in Hf more than in α-Zr and α-Ti. Any difference in the effect of oxygen on the diffusion of metal solutes between α-Ti and α-Zr could be due only to a larger Hägg parameter λ in α-Ti as compared with α-Zr.

4.4. Interstitial solute–vacancy pair and interstitialcy mechanisms

For the fast diffusion in the solute–solvent system Cd–Pb the 'interstitial solute–vacancy pair model' has been developed [93]. In fact, this model is relatively close to the Hägg model but since it is based mainly on thermodynamic arguments it lacks the geometrical frame of the latter. The role of the vacancies may be overemphasized and the role of the various interactions is neglected, see Section 4.2.2.

The interstitialcy model originally proposed for interstitial Ag self-diffusion in AgBr is here rather unlikely. In α-Zr it is very doubtful that a small interstitial solute in its octahedral site should be able to push a large adjacent Zr lattice atom into the next octahedral site and take its lattice position. Yet, under irradiation this mechanism may become possible for 3d-solutes. The solute ion should then regain (part of) its valence electrons when it enters the lattice position. Interstitial oxygen atoms should behave differently.

As regards the fcc non-transition host metal Pb [62–64,94], a correlation between Q and λ exists for Cu, Au, Ag and Cd in this order (see Table 3(c)), but only Cd carries its normal valence $z = 2$ whereas Cu and Ag have $z = 2$ instead of 1 and Au might adopt even $z = 3$ instead of 1. Thus, these experiments and other related ones require a more detailed analysis along the lines of Section 2.1 and Figs. 1 and 2. This is not attempted here.

4.5. Hägg approach and Miedema model

Some years ago Bakker [11] published an analysis of fast diffusion in the host phases, Pb, γ-U, Pr and other host metals. Similar to previous authors Bakker rejected the possibility that Hägg's rule and the associated HSM could be applied to this problem and based his analysis on the Miedema model [95,96]. The use of the Miedema model for analysing fast diffusion in dilute binary alloys is certainly possible and, in fact, Bakker's results with regard to fast diffusion in γ-U and Pb are similar to those in the present paper. One can identify his ratio V_{imp}/V as a parameter which resembles the Hägg parameter λ although it has a different physical meaning. Incidently the numerical values are partly similar and partly even very close and also the critical Hägg value $\lambda = 0.59$ seems to be numerically the same for Bakker's volume ratio V_{imp}/V. In fact, this is not too surprising because the attribution of the effective valences z_e with the associated ionic radii $R_I(z_e)$ to the solute atoms in the Hägg approach corresponds to Bakker's 'volume contraction when a metal impurity is introduced into a metal' [11]. The advantage of the Hägg approach resides in Eq. (3), i.e., in the separation of Q into the elastic saddle point energy and the chemical interaction. Based on the Wigner–Seitz approach the Miedema model very successfully treats the heats of solution and the heats of formation of intermetallic compounds for binary alloys. This is achieved by formulating a schematized chemical interaction between the valence electrons of the alloy constituents on a semi-empirical basis neglecting the structural details which are just taken into account by the Hägg approach. Hence Miedema model and Hägg approach are in a certain way complementary.

4.6. Enhanced self-diffusion and fast solute diffusion in the bcc phase of γ-Zr and of γ-U

4.6.1. Diffusion in β-Zr

The effect of the polyvalent substitutional solutes Nb and Mo on self-diffusion has been discussed in detail within the frame of the anomalous self-diffusion in β-Zr, β-Ti and β-Hf and its physical origin, the softening of the LA $2/3\langle 111\rangle$ mode in the lattice vibrations of these bcc phases when approaching the β/α transition (see Ref. [5] and the literature cited there, e.g., Refs. [3,97]). The interaction between the 4d-electrons of Nb and Zr affects this mode and explains the lowering of the coefficient for self-diffusion in β-Zr by Nb, D_1(Nb), in the lower temperature range of the β-Zr phase field if β-Zr is alloyed with Nb. The fact that the ratio of the diffusion coefficients for tracer diffusion of Nb D_2^0 and of self-diffusion D_1^0 in β-Zr is 1:5 at 40 K above transition and about 1:1 at high temperatures [29,55] can be attributed to the same cause.

As regards the substitutionally diffusing solutes belonging to the Hägg class of dilute alloys ($z \leq 2$) with $\lambda > 0.59$, V and Ag (see Table 3(a)), their tracer diffusion coefficients show a curvature similar to the coefficient of self-diffusion in β-Zr. This is indicated in Table 3(a) by the two Q-values, with the higher one at the higher temperature range.

However, evidence for curved Arrhenius plots of the fast diffusing 3d-solutes with $\lambda < 0.59$ does not exist for Fe up to 1880 K and for Co up to 1740 K [29]. Curvature may, however, exist for Co at $T > 1800$ K [56]. In conclu-

sion any curvature, i.e., interaction between interstitial solutes and the LA $2/3\langle 111\rangle$ mode in β-Zr, appears hardly to exist or must be much weaker than for metallic solutes diffusing by the vacancy mechanism.

4.6.2. Diffusion in γ-U

The bcc phase of uranium showing anomally high self-diffusion is expected to possess also the soft LA $2/3\langle 111\rangle$ mode. Axe et al. [98] discuss a possible 'freezing-in' of TA soft phonons for the direct γ/α transformation in U which occurs under pressure [87]. A description of the γ/β transformation becomes rather complex [99]. Inelastic phonon scattering could not yet be studied in γ-U because of experimental problems [100].

Because of the limited temperature range of the γ-U phase, spanning only $0.745 < T/T_m < 1.00$, curvature in Arrhenius plots of the coefficient of self-diffusion would be difficult to detect but the similarities with the binary dilute alloy systems of the β-Zr host yield some information. Like the system Zr–Nb also the bcc phase of binary U–Zr alloys shows complete mutual solid solubility and the behaviour of small additions of Nb to β-Zr and to γ-U should thus affect diffusion in the same way. This is in fact the case, as can be deduced from the data in Table 1(a) [34]. Analogous to Nb in β-Zr (see Table 3(a) and part I), the ratio $D_1^0{:}D_{Nb}^0$ in α-U is even larger, 10:1 about 15 K above the transition, and this ratio reduces to 2.8:1 at 0.97 T_m. Hence the anticipated LA $2/3\langle 111\rangle$ mode in bcc γ-U is also affected by Nb as in β-Zr [101]. In γ-U the interaction with the 4d-electrons of Nb very probably involves 5f-electrons besides the 6d-electrons, see Fig. 2. This may be the reason for the larger ratio $D_1^0{:}D_{Nb}^0$ in γ-U than in β-Zr. The similarity between the two host phases is found roughly also in alloys between γ-U and 10 at.% Zr, Mo and Nb, see Fig. 5 taken from Ref. [102]. Alloying γ-U with 10 at.% Zr changes the self-diffusion in γ-U little, with 10 at.% Mo considerably and with 10 at.% Nb even more.

As regards the Hägg class solutes with $z \leq 2$, Cu and Au possess $\lambda > 0.59$ and are substitutional diffusers in γ-U. In analogy to V in β-Zr which certainly diffuses by the vacancy mechanism because of its curved Arrhenius plot (see Table 3(a)), one would expect V (no experimental data available in γ-U) to show $z = 1$ instead of 2, adopt $\lambda > 0.59$ and migrate also by the vacancy mechanism as suggested in Table 1(a).

This leaves a last anomaly to be mentioned which has been found for all solutes examined in γ-U [34,35]. Within 50 K of the γ/β transition the Arrhenius plots of all solutes present in Fig. 3 and Table 1a possess a slight positive curvature. This effect had been carefully examined by the authors of Ref. [34] and remained unexplained. The otherwise close resemblance of solute diffusion and self-diffusion between γ-U and β-Zr suggests when approaching the γ/β transition that in uranium the similarity with β-Zr must end because γ-U does not transform into the hcp structure of a normal metal but into the complicated structure indicated in Section 2.2.3. Hence the transformation cannot be prepared by the soft phonen modes L $(2/3)\langle 111\rangle$ and T_1 $(1/2)\langle 110\rangle$ [5,98]. Perhaps a clue to the structure of the β-U phase nuclei in γ-U may be that the bcc lattice may be regarded as a distorted structure with CN 14 and also β-U possesses CN 14.

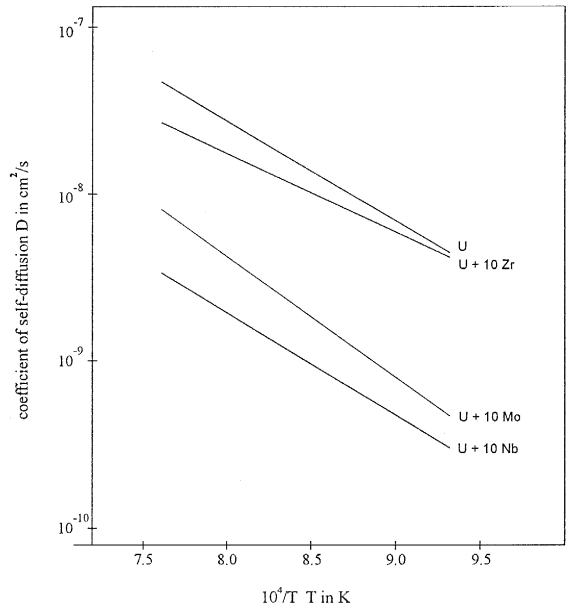

Fig. 5. The effect of alloying γ-U with 10 at.% Zr, Mo and Nb, respectively, on the coefficient of self-diffusion of γ-U. Note the small effect of Zr and the large effects of Mo and Nb [102]. See discussion in Section 4.6.2.

5. Summary and conclusion

Based on the previously established modified Hägg rule [13] this empirical approach has been extended to the analysis and comparison of published data on fast diffusion in a special class of dilute binary alloys for the host phases β- and γ-U, α- and β-Zr, Nb and in a preliminary way Pb. In this way information from five aspects of solid state science can be brought qualitatively into a coherent picture:

- Discrimination between systems with fast and with normal diffusion on the basis of the Hägg parameter λ.
- The detailed geometry of the lattice structure of the host phases by the hard sphere model.
- The electronic properties of the free solvent and solute atoms.
- The relevant binary phase diagrams.
- The elastic properties of the host phases.

In particular the activation enthalpy Q of fast solid diffusion is resolved into elastic contributions related to λ

and electronic contributions. The anisotropy of fast diffusion in hcp lattices can be understood on this basis. The special roles of Fe and O are explained as regards solute–host interactions. The general trend in fast diffusion behaviour in the other group IV host metals α-Ti and α-Hf are predicted from the comparison of the relevant binary solute–solvent phase diagrams. Chemical solute–solvent interaction, solute valences and related Hägg parameters λ can be understood in a zeroth order approximation by comparing the energies of the valence electron states between host atoms and solute atoms. In bcc host phases two slightly different interstitial mechanisms have been identified, depending on a critical Hägg parameter λ_c and solutes either occupy tetrahedral or octahedral interstices in the bcc lattice.

In the 'anomalous' bcc phases γ-U and β-Zr a noticeable interaction between enhancement of self-diffusion and fast interstitial diffusion does not exist.

The Hägg approach is compared with the interstitial-vacancy pair model of Miller and the Miedema model. Both models are partly complementary to the Hägg approach but lack the necessary geometrical conditions of the latter.

In conclusion the present paper provides a new frame for the development of the quantitative physics of fast diffusion along general directions outlined in Ref. [103] for the various aspects of normal diffusion. The latter work came to the notice of the author when this paper had been finished.

Acknowledgements

A discussion of the density functional theory with M.S.S. Brooks, EITU Karlsruhe, is acknowledged. A. Lawson of Los Alamos Nat. Lab. and G.H. Lander of EITU kindly provided the list of bond lengths in β-U from which the average model radius $\overline{R}_M$ for this phase in Table 1b has been deduced. Last but not least the author would like to thank J.L. Bocquet of C.E. Saclay, for providing a reprint of Ref. [103] and for comments on Ref. [13] as regards Ref. [91].

References

[1] A.D. Le Claire, J. Nucl. Mater. 69&70 (1978) 70.
[2] C. Herzig and U. Köhler, Acta Metall. 35 (1987) 1831.
[3] C. Herzig and U. Köhler, Mater. Sci. Forum 15–18 (1987) 301; Philos. Mag. A58 (1988) 769.
[4] W. Petri and G. Vogl, Mater. Sci. Forum 15–18 (1987) 323.
[5] A. Heiming, W. Petri, J. Trampenau, M. Alba, C. Herzig, H.R. Schober and G. Vogl, Phys. Rev. B43 (1991) 10948.
[6] B. Sepiol and G. Vogl, Phys. Rev. Lett. 71 (1993) 731.
[7] G.M. Hood, Defect Diffusion Forum 95–98 (1993) 755.
[8] G.M. Hood, H. Zou, D. Gupta and R.J. Schultz, J. Nucl. Mater. 223 (1995) 122.
[9] G. Vogl, Hyperfine Interact. 53 (1990) 197.
[10] Y. Yoshida, M. Sugimoto, D. Tuppinger and G. Vogl, Defect Diffusion Forum 66–69 (1989) 347.
[11] H. Bakker, J. Less-Common Met. 105 (1985) 129.
[12] R. Tendler and J.P. Abriata, J. Nucl. Mater. 150 (1987) 251.
[13] H. Blank, Philos. Mag. B73 (1996) 833.
[14] T.R. Anthony, J.W. Miller and D. Turnbull, Scr. Metall. 3 (1969) 183.
[15] G. Hägg, Z. Phys. Chem. B6 (1929) 221; B12 (1931) 23.
[16] L.H. Ahrens, Geochim. Cosmochim. Acta 2 (1952) 155.
[17] R.C. Weast, ed., Handbook of Chemistry and Physics, 70th Ed. (CRC, Boca Raton, FL, 1989) p. F-187.
[18] R.D. Shannon and C.T. Prewitt, Acta Crystallogr. B25 (1969) 925.
[19] D.D. Shannon, Acta Crystallogr. A32 (1976) 751.
[20] F.G. Fumi and M.P. Tosi, J. Phys. Chem. Solids 25 (1964) 31, 45.
[21] J.A. Van Vechten and J.C. Phillips, Phys. Rev. B2 (1970) 2160.
[22] V.L. Moruzzi, J.K. Janak and A.R. Williams, Calculated Electronic Properties of Metals (Pergamon, New York, 1978).
[23] M.S.S. Brooks and B. Johansson, in: Handbook of Magnetic Materials, ed. K.H.J. Buschow, Vol. 7 (Elsevier Science, Amsterdam, 1993) ch. 3, p. 139.
[24] F. Herman and S. Skillman, Atomic Structure Calculations (Prentice-Hall, Eaglewood Cliffs, NJ, 1963).
[25] J.P. Desclatux and A.J. Freeman, in: Handbook on the Physics and Chemistry of the Actinides, eds. A.J. Freeman and G.H. Lander, Vol. 1 (North-Holland, Amsterdam, 1984) ch. 1, p. 1.
[26] D.G. Pettifor, Bonding and Structure of Molecules and Solids (Clarendon, Oxford, 1995).
[27] H.W. King, in: Physical Metallurgy, Pan 1, eds. R.W. Cahn and P. Haasen (North-Holland Physics, Amsterdam, 1983) p. 37.
[28] G.P. Partridge, Metall. Rev. 12 (1967) 169.
[29] C. Herzig, J. Neuhaus, K. Vieregge and L. Manke, Mater. Sci. Forum 15–18 (1987) 481.
[30] W.B. Pearson, The Crystal Chemistry and Physics of Metals and Alloys (Wiley-Interscience, New York, 1972).
[31] A.C. Larson, C.E. Olsen, J.W. Richardson Jr., M.H. Mueller and G.H. Lander, Acta Crystallogr. B44 (1988) 89.
[32] G. Bergman and D.P. Shoemaker, Acta Crystallogr. 7 (1954) 857.
[33] C.F. Frank and J.S. Kaspar, Acta Crystallogr. 11 (1958) 184; 12 (1959) 483.
[34] N.L. Peterson and S.J. Rothman, Phys. Rev. 136 (1964) A 842.
[35] S.J. Rothman, J. Nucl. Mater. 3 (1961) 77.
[36] Y. Adda, A. Kirianenko and C. Mairy, J. Nucl. Mater. 1 (1959) 300.
[37] S.J. Rothman, J. Gray, J.P. Hughes and A.L. Harkness, J. Nucl. Mater. 3 (1961) 72.
[38] A.A. Bochvar, V.G. Kuznetsova, V.S. Sergeev and F.P. Butra, At. Energ. 18 (1965) 601.
[39] S.J. Rothman, N.L. Peterson and S.A. Moore, J. Nucl. Mater. 7 (1962) 212.

[40] M.P. Dariel, M. Blumenfeld and G. Kimmel, J. Appl. Phys. 41 (1970) 1480.
[41] K.H. Eckelmeyer, M.O. Eatough and M.E. McAllaster, J. Nucl. Mater. 170 (1990) 157.
[42] F. Dyment and C.M. Libanati, J. Mater. Sci. 3 (1968) 349.
[43] R.P. Agarwala, S.P. Murarka and M.S. Anant, Acta Metall. 16 (1968) 61.
[44] S.N. Balart, N. Varela and R.H. Tendler, J. Nucl. Mater. 119 (1983) 59.
[45] H. Nakajima, G.M. Hood and R.J. Schultz, Philos. Mag. B58 (1988) 319.
[46] G.V. Kidson, Philos. Mag. A44 (1981) 341.
[47] G.M. Hood and R.J. Schultz, Mater. Sci. Forum 15–18 (1987) 475.
[48] G.M. Hood and R.J. Schultz, Phys. Rev. B11 (1975) 3780.
[49] K. Vieregge and C. Herzig, J. Nucl. Mater. 165 (1989) 65.
[50] G.M. Hood, H. Zou, S. Herbert and R.J. Schultz, J. Nucl. Mater. 210 (1994) 1.
[51] I.G. Ritchie and A. Atrens, J. Nucl. Mater. 67 (1977) 254.
[52] D. Quataert and F. Coen-Porisine, J. Nucl. Mater. 36 (1970) 20.
[53] R.H. Tendlet and C.F. Varotto, J. Nucl. Mater. 46 (1973) 107.
[54] G.M. Hood and R.J. Schultz, Zirconium in the Nuclear Industry: 8th. Int. Symp. STP 1023 (ASTM, Philadelphia, PA, 1989) p. 435.
[55] J.I. Federer and T.S. Lundy, Trans. Metall. Soc. AIME 227 (1963) 592.
[56] G.V. Kidson and G.J. Young, Philos. Mag. 20 (1969) 1047.
[57] Y. Yoshida, W. Mieckeley, W. Petri, R. Stehr, K.H. Steinmetz and G. Vogl, Mater. Sci. Forum 15–18 (1987) 487.
[58] L.I. Nicolai and R.H. de Tendler, J. Nucl. Mater. 87 (1979) 401.
[59] L. Manke and C. Herzig, Acta Metall. 30 (1982) 2085.
[60] L.V. Pavlinov, A.I. Nakonechnikov and N. Bykov, At. Energ. 19 (1965) 1495.
[61] D. Ablitzer and A. Vignes, J. Nucl. Mater. 69&70 (1978) 97.
[62] B.F. Dyson, T. Anthony and D. Turnbull, J. Appl. Phys. 37 (1966) 2370.
[63] J.W. Miller, Phys. Rev. 181 (1969) 1095.
[64] A. Ascoli, E. Germagnioli and L. Mougin, Nuovo Cim. 4 (1956) 123.
[65] J.P. Abriata and J.C. Bolcich, Bull. Alloy Phase Diagrams 3 (1982) 33.
[66] J.F. Smith, Phase Diagrams of Binary Vanadium Alloys (ASM, Materials Park, OH, 1989).
[67] H. Okamoto, J. Phase Equil. 14 (1993) 768.
[68] R.P. Elliott, Constitution of Binary Alloys (McGraw-Hill, New York, 1965) Suppl. 1, p. 621.
[69] F. Aubertin, U. Gonser, S.J. Campbell and H.-G. Wagner, Z. Metallkd. 76 (1985) 237.
[70] H. Zou, G.M. Hood, H. Nakajima, J.A. Ray, R.J. Schultz and J.A. Jackman, J. Nucl. Mater. 210 (1994) 239.
[71] D. Arias and J.P. Abriata, Bull. Alloy Phase Diagrams 9 (1988) 597.
[72] T.O. Malakhova and A.N. Kobylkin, Russ. Metall. 2 (1982) 187.
[73] W.H. Pechim, D.E. Williams and W.L. Larsen, Trans. ASM 57 (1964) 464.
[74] H. Zou, G.M. Hood, H. Nakajima, J.A. Ray and R.J. Schultz, J. Nucl. Mater. 223 (1995) 186.
[75] P. Nash and C.S. Jayanth, Phase Diagrams of Binary Ni Alloys (ASM International, Materials Park, OH, 1991) p. 390.
[76] D. Arias and J.P. Abriata, Bull. Alloy Phase Diagrams 11 (1990) 452.
[77] J.P. Abriata, J. Garces and R. Versaci, Bull. Alloy Phase Diagrams 7 (1986) 116.
[78] I. Karakaya and W.T. Thompson, J. Phase Equil. 13 (1992) 143.
[79] T.B. Massalski, H. Okamoto and J.P. Abriata, Bull. Alloy Phase Diagrams 6 (1985) 519.
[80] R.P. Elliott, Constitition of Binary Alloys (McGraw-Hill, New York, 1965) Suppl. 1, p. 858.
[81] H. Blank, Z. Metallkd. 85 (1994) 645.
[82] M. Lubbehusen, K. Vieregge, G.M. Hood, H. Mehrer and Chr. Herzig, J. Nucl. Mater. 182 (1991) 164.
[83] C. Hellio, H.H. de Novion, A. Marraud and L. Boulanger, Mater. Sci. Forum 15–18 (1987) 936.
[84] A.D. King, G.M. Hood and R.A. Holt, J. Nucl. Mater. 185 (1991) 174.
[85] M. Köppers, Chr. Herzig, U. Södervall and A. Lodding, Defect Diffusion Forum 95–98 (1993) 783.
[86] W. Frank, Philos. Mag. A63 (1991) 897.
[87] W. Klement Jr., A. Jayaraman and G.C. Kennedy, Phys. Rev. 129 (1963) 1971.
[88] P.E. Armstrong, D.T. Eask and J.E. Hockett, J. Nucl. Mater. 45 (1972/1973) 211.
[89] E.S. Fisher and C.J. Renken, Phys. Rev. A135 (1964) 482.
[90] J. Ashkenazi, M. Dacorogna, M. Peter, Y. Talmor and E. Walker, Phys. Rev. B18 (1978) 4120.
[91] P.A. Varotsos and K.D. Alexopoulos, Thermodynamics of Point Defects and Their Relation with Bulk Properties (North-Holland, Amsterdam, 1986).
[92] H. Nakajima and M. Koiwa, Defect Diffusion Forum 95–98 (1993) 775.
[93] J.W. Miller, Phys. Rev. 188 (1969) 1074.
[94] J.B. Hudson, Trans. Metall. Soc. AIME 221 (1961) 761.
[95] A.R. Miedema, P.F. de Chatel and F.R. de Boer, Physica B100 (1980) 1.
[96] A.R. Miedema and A.K. Niessen, Physica B114 (1982) 367.
[97] W. Petfi, A. Heiming, J. Trampenau and G. Vogl, Defect Diffusion Forum 66–69 (1989) 157.
[98] J.D. Axe, G. Grübel and G.H. Lander, J. Alloys Compd. 213 (1994) 262.
[99] B. Mettout, V.P. Dmitriev, M.B. Jaber and P. Toledano, Phys. Rev. B48 (1993) 6908.
[100] G.H. Lander, private communication (1996).
[101] K.-M. Ho, C.L. Fu and B.N. Harmon, Phys. Rev. B29 (1984) 1575.
[102] Y. Adda, A. Kirianenko and M. Bandazzoli, C.R. 253 (1961) 613.
[103] J.L. Bocquet, G. Brebec and Y. Limoge, in: Physical Metallurgy, 4th revised and enhanced Ed., eds. R.W. Cahn and P. Haasen (North-Holland, Amsterdam, 1996) ch. 7.